

1
2
3
4
5
6
7
8
9
10
11
12
13
14
15
16
17
18
19
20
21
22
23
24
25
26
27
28
29
30
31
32
33
34
35
36
37
38
39
40
41
42
43
44
45
46
47
48
49
50
51
52
53
54
55
56
57
58
59
60
61
62
63
64
65

**A neutron diffraction study of the oxygen diffusion in molybdenum doped
 $\text{Ba}_2\text{In}_2\text{O}_5$**

Aurélie Rolle^{a}, Pascal Roussel^a, Nambi Venkatesan Giridharan^a,
Emmanuelle Suard^b, Rose-Noëlle Vannier^a*

^a *Equipe de Chimie du Solide – UCCS – Unité de Catalyse et Chimie du Solide – UMR 8181
USTL-ENSCL, BP 90 108, 59652 Villeneuve d’Ascq Cedex, France*

^b *Institut Laue Langevin, Avenue des martyrs, BP 156, 38042 Grenoble Cedex 9, France*

* Corresponding author

Dr. A. Rolle

Equipe de Chimie du Solide, UCCS – Unité de Catalyse et Chimie du Solide

CNRS UMR 8181, USTL-ENSCL, BP 90 108, 59 652 Villeneuve d’Ascq Cedex, France

Tel: +33 (0) 3 20 43 49 73

Fax: +33 (0) 3 20 43 68 14

E-mail: Aurelie.Rolle@ensc-lille.fr

1
2
3
4 **Abstract**
5
6
7

8
9 The structures of molybdenum doped $Ba_2In_2O_5$ were refined using X-ray and neutron
10 diffraction data at room and high temperature with the aim to derive preferred oxygen diffusion
11 pathways. At room temperature, refinement of composition $Ba_2In_{2-x}Mo_xO_{5+3x/2}$ with $x=0.1$
12 revealed molybdenum atoms are preferentially located in the tetrahedral layers of the
13 brownmillerite. At $700^\circ C$, the structure can be viewed as the stacking of alternating In and In/Mo
14 octahedral layers. The conduction process occurs preferentially in the later which is highly
15 oxygen deficient. Preferred oxygen diffusion pathways were deduced from Joint Probability
16 Density Function (JPDF) and energy barriers were derived. It was in good agreement with the
17 activation energy deduced from impedance spectroscopy for composition $x=0.1$ at $950^\circ C$.
18 However, calculation of energy barrier assumes a dynamic disorder of oxide ions which is
19 unlikely to occur at lower temperature and for sample containing a larger amount of
20 molybdenum. Composition $x=0.5$ is cubic on the whole range of temperature. At room
21 temperature, JPDF revealed a static disorder of the oxygen atoms, which is likely due to the
22 solution of molybdenum into the barium indium perovskite. When temperature increases the
23 disorder becomes more and more dynamic.
24
25
26
27
28
29
30
31
32
33
34
35
36
37
38
39

40 **Keywords**

41
42 Barium oxide, indium oxide, brownmillerite, oxide ion conductor, neutron diffraction, X-ray
43 diffraction, anharmonic model
44
45
46
47
48
49
50
51
52
53
54
55
56
57
58
59
60
61
62
63
64
65

1. Introduction

In 1990, Goodenough *et al.* evidenced high oxide ion conduction properties in the high temperature forms of the $\text{Ba}_2\text{In}_2\text{O}_5$ [1]. Since then, numerous substitutions for the indium site or for the barium site have been made to stabilise these conductive forms at lower temperature.

At room temperature, the structure of $\text{Ba}_2\text{In}_2\text{O}_5$ is similar to that of the brownmillerite which can be described as a defective perovskite. Its symmetry is orthorhombic with the following unit-cell: $a_B = \sqrt{2} a_P = 6.0991 \text{ \AA}$, $b_B = 4a_P = 16.7365 \text{ \AA}$, $c_B = \sqrt{2} a_P = 5.9622 \text{ \AA}$ (a_P , b_P , c_P corresponding to the perovskite cell) [2]. It can be viewed as an intergrowth of $\text{In}(1)\text{O}_6$ octahedral layers alternating with $\text{In}(2)\text{O}_4$ tetrahedral layers, barium atoms being located in the B site of the perovskite. This orthorhombic form changes to a tetragonal polymorph at $T_d \approx 925^\circ\text{C}$. As the temperature increases, the oxygen disorder increases. For temperatures higher than 1040°C , $\text{Ba}_2\text{In}_2\text{O}_5$ transforms to an oxygen deficient perovskite with cubic symmetry which can be described in the $Pm\bar{3}m$ space group. These two high temperature (tetragonal and cubic) forms are pure oxide ion conductors [3-9] and were tentatively stabilised at room temperature by partial substitution for barium and/or indium. Our group investigated the partial substitution for indium with high valence state metals. Tin, vanadium, niobium, tantalum, molybdenum and tungsten were considered. Solid solutions were evidenced for all the tested metals [10, 11]. In the case of molybdenum, a $\text{Ba}_2\text{In}_{2-x}\text{Mo}_x\text{O}_{5+3x/2}$ solid solution was obtained for $0 \leq x \leq 2/3$, up to the complete filling of the oxygen vacancies of the perovskite. Cubic forms were stabilised at room temperature for composition with $x \geq 0.2$. For the orthorhombic polymorph obtained with lower x value, impedance spectroscopy and high temperature X-ray diffraction revealed a decrease of the order-disorder transition temperature with the increase of the substitution level. But the fast oxide ion conductivity decreased with the increase of the substitution rate. Composition $x=0.1$ is orthorhombic at room temperature, it transforms to a tetragonal form at 600°C and its symmetry becomes cubic at 925°C . The Arrhenius plot, $\log(\sigma T) = A \exp(-E_a/kT)$, derived from the data reported in [10], is given in Fig. 1. The transition from the tetragonal form to the cubic form is not clearly visible. In the case of composition $x=0.1$, an activation energy of 1eV was deduced at temperature higher than 600°C . It was 0.8eV for composition $x=0.5$ for temperature higher than 600°C .

1
2
3
4 From a structural point of view, the dopant location in the brownmillerite type structure is
5 not trivial. In the orthorhombic polymorph, there are two possibilities. They can substitute either
6 the In(1) site, located in the octahedral layers (1) or the In(2) site, located in the tetrahedral layers
7 (2). Moreover, the substitution of indium by a cation with valence higher than 3 should induce the
8 introduction of interstitial oxygen atoms in the brownmillerite type structure. To define the
9 position of the molybdenum atoms and extract information on the mechanisms of oxygen
10 transport in the $\text{Ba}_2\text{In}_{2-x}\text{Mo}_x\text{O}_{5+3/2x}$ solid solution, X-ray and neutron diffraction data were
11 collected at several temperatures for composition $x=0.1$ and $x=0.5$. A high disorder of oxide ions
12 was observed and preferred oxygen pathways were deduced from the analysis of the Probability
13 Density Function of oxygen nucleon.
14
15
16
17
18
19
20
21
22
23
24
25

26 2. Experimental

27
28 $\text{Ba}_2\text{In}_{2-x}\text{Mo}_x\text{O}_{5+3/2x}$ $x=0.1$ and $x=0.5$ compositions were prepared by classical solid-state
29 route from stoichiometric mixtures of In_2O_3 (Aldrich, 99.99%), BaCO_3 (Aldrich 99%), MoO_3
30 (Prolabo, 99-100%) reagents at 1000°C, 1200°C and 1300°C with intermediate grindings [10].
31 Powders were dried at 500°C for 1 hour (heating rate: 10°C/min, cooling rate: 20°C/min) under a
32 flow of dried air to avoid any traces of hydrates before the data collection. Both compositions
33 were checked by EDX analysis before further characterisations. The experiments were performed
34 on a Jeol 5300 scanning electron microscope equipped with a Princeton Gamma Technology
35 energy dispersive detector. $\text{Ba}_2\text{In}_2\text{O}_5$ and MoO_3 were used as references. It led to the following
36 compositions: $\text{Ba}_2\text{In}_{1.90}\text{Mo}_{0.10}\text{O}_{5.15}$ and $\text{Ba}_2\text{In}_{1.49}\text{Mo}_{0.51}\text{O}_{5.76}$ in very close agreement with the
37 starting compositions and confirmed there had been no volatilisation of molybdenum.
38
39
40
41
42
43
44
45
46

47 Neutron diffraction data were collected at room temperature on the high resolution
48 powder diffractometer D2B at the Institut Laue Langevin (I.L.L.) at Grenoble. To perform
49 collection under air atmosphere, approximately 20g of powder were introduced in a quartz tube,
50 which was open at one end. This tube was introduced in the furnace and data were collected in
51 the 0.3-160° range with a step of 0.05°. Collection was performed at room temperature, 700°C
52 and 950°C for composition $x=0.1$ and room temperature and 750°C for composition $x=0.5$.
53
54
55
56
57
58
59
60
61
62
63
64
65

1
2
3
4 X-ray diffraction data were collected at room temperature on a Bruker axs D8 Advance
5 diffractometer equipped with a solX energy dispersive detector in the 5-100° range with a step of
6 0.02° and a counting time of 25 seconds per step ($\text{Cu}_{K\alpha}=1.54 \text{ \AA}$). The high temperature
7 diffraction data were collected in the 9-100° range, with a step of 0.015° and a counting time of
8 0.2 seconds per step, on a Bruker axs D8 Advance diffractometer equipped with a high
9 temperature Anton Paar HTK 1200 N chamber and a one dimensional X-ray detector VÅNTEC-1
10 ($\text{Cu}_{K\alpha}=1.54 \text{ \AA}$).
11
12
13
14
15
16
17

18 The JANA 2000 software [12], option powder, was used for the structural refinement
19 from the X-ray and neutron diffraction data. The Rietveld method was applied. The profile was
20 described by a pseudo-Voigt function and the background was determined manually. The
21 software WxDragon 1.1.4. [13] was used to represent the probability density functions in three
22 dimensions.
23
24
25
26
27
28
29

30 **3. Results and discussions**

31 *3.1. Composition $x=0.1$ at room temperature*

32
33
34
35
36 The orthorhombic symmetry of composition $x=0.1$ was confirmed by X-ray diffraction.
37 However, because of the close atomic numbers of In ($Z=49$) and Mo ($Z=42$), it was not possible
38 to define clearly in which site the substituting metal was located using X-ray data only. A better
39 separation was expected with neutron diffraction, Fermi lengths being 4.06 fm and 6.9 fm for
40 indium and molybdenum, respectively. The wavelength of neutron being not accurate, it was
41 refined with the unit cell parameters of this composition constrained to the value obtained from
42 X-ray diffraction data. This led to a value of $\lambda = 1.59483(2)\text{\AA}$.
43
44
45
46
47
48

49 To describe the brownmillerite type structure, several structural models were reported in
50 the literature. $\text{Ca}_2\text{Fe}_2\text{O}_5$ was described in *Pcmn* [15] and $\text{Ba}_2\text{In}_2\text{O}_5$ in *Ibm2* [14] and *Icmm* [2]
51 space groups. The structural models in *Ibm2* and *Pcmn* differ from the orientation of the $\text{In}(2)\text{O}_4$
52 tetrahedra (Fig. 2) in the oxygen deficient layers and, as shown by Berastegui using TEM [2], the
53 reality is likely a mixture of these different configurations. Therefore, the structure is better
54 described in the *Icmm* which can be considered as the superimposition of these two later models.
55
56
57
58
59
60
61
62
63
64
65

1
2
3
4 In this space group, In(2) and O(3) sites are located in a (8i) site with a partial occupancy of 0.5
5 which allows two possible orientations for the tetrahedra in the In(2)O layers (Fig. 3).

6
7 Thus, data collected at room temperature were refined using the model proposed by Berastegui
8 [2]. Molybdenum was first introduced in both In(1) and In(2) sites with a constrain on their
9 occupancy to verify the initial composition. Occupancies were refined in the last step of the
10 refinement. It led to a negative occupancy for molybdenum in the In(1) site (-0.022(8)) and
11 clearly converged in the In(2) site. Molybdenum was therefore introduced in the In(2) site and its
12 occupancy was fixed to 0.05 to verify the stoichiometry. As a result, molybdenum is located in
13 the oxygen deficient layers of Ba₂In₂O₅. At this stage a Fourier difference was calculated and
14 revealed an extra oxygen position at (1/4, 1/4, 1/4). This extra oxygen site was then introduced in the
15 refinement and occupancies of all oxygen sites were refined with a constrain on the sum of their
16 occupancies to be equal to the expected oxygen stoichiometry. The structural model deduced
17 from neutron diffraction was then tentatively refined using the X-ray diffraction data. Because of
18 the low oxygen scattering factors, their positions were constrained to the values obtained from
19 neutron diffraction. The derived positions were the same within the error.
20
21
22
23
24
25
26
27
28
29
30

31 The calculated profiles compared to experimental data are given in Fig. 4. A good
32 agreement between the calculated profiles and the experimental data was observed as confirmed
33 by the reliability factors. The corresponding structural model is reported in Table 1. As expected,
34 the extra oxygen atoms introduced by the substitution are also located in the oxygen defective
35 layers. The O(2) site, which corresponds to the apical site of the perovskite layers, is fully
36 occupied. The O(1) site, located in the equatorial plane of the octahedral layers, is almost fully
37 occupied, whereas vacancies are clearly evidenced on the O(3) site, located in the equatorial plane
38 of the oxygen deficient layers.
39
40
41
42
43
44
45
46
47

48 3.2. Composition $x=0.1$ at 700°C 49

50
51 At 700°C, X-ray diffraction confirmed the tetragonal symmetry of this composition. The
52 structure of the tetragonal polymorph of Ba₂In₂O₅ was tentatively described by Speakman *et al.* in
53 the following unit cell $a_T=b_T=a_B=\sqrt{2} a_P$ and $c_T=b_B=4a_P$ [9]. They obtained the best agreement
54 factors in the *I4cm* space group. However, a rapid analysis of the coordinates of atoms revealed
55 some correlations between positions and questioned the quadrupling of the stacking parameters.
56
57
58
59
60
61
62
63
64
65

1
2
3
4 In fact, the structure of $\text{Ba}_2\text{In}_2\text{O}_5$ derivatives with a tetragonal symmetry was described by
5 numerous authors in a double perovskite with $c_T=2a_P$ [14, 16-19]. The double perovskite was also
6 confirmed by TEM by Jayaraman *et al.* [20], Liu *et al.* [21] and Kambe *et al.* [22] for $\text{Ba}_2(\text{In}_{1-x}\text{Ti}_x)_2\text{O}_5$,
7 $(\text{Ba}_{1-x}\text{La}_x)_2\text{In}_2\text{O}_{5+x}$ and $\text{Ba}_2\text{InCuO}_{4.53}$, respectively. In their paper, Speakman *et al.* gave
8 no evidence of a quadrupling of the perovskite unit-cell along the [001] direction and the high
9 temperature tetragonal form of $\text{Ba}_2\text{In}_2\text{O}_5$ is likely a double perovskite composed of two octahedral
10 layers, one being oxygen defective.
11
12
13
14
15
16
17

18 Neutron diffraction data were therefore refined in the $P4/mmm$ space group, assuming a
19 double perovskite unit-cell. The wavelength of the neutron being known from the experiment
20 performed at room temperature, unit cell parameters were refined. It led to parameters very close
21 to those derived from X-ray diffraction (Table 2). No extra Bragg peaks was observed, either on
22 the X-ray patterns, or on the neutron patterns. Due to the fast oxygen motion, a large disorder of
23 oxide ions was noticed in the oxygen deficient layers. To take into account all the nuclear density
24 of O(2) and O(3) oxygen atoms, an anharmonic description of the thermal parameters at the 4th
25 order was used. The Hamilton test [23] was carried out to compare the anharmonic description
26 (27 refined parameters, 92 reflexions) to the model with an anisotropic description of the thermal
27 motion of oxygen atoms (15 refined parameters, 92 reflexions). This led to the following
28 reliability factor for the anharmonic model: Robs: 2.55, Rwpbs: 1.39, compared to Robs: 4.04,
29 Rwpbs: 2.33 for the anisotropic model. Statistical calculations revealed that the anharmonic
30 description is better than the anisotropic description with a 995/1000 probability. In contrast,
31 thermal displacement of barium, indium, molybdenum and oxygen O(1) atoms could be fitted
32 using classical anisotropic parameters. Refinement of the molybdenum occupancy in both indium
33 sites confirmed it was located in the In(2) site. Refinement of the oxygen atoms occupancy
34 revealed the apical O(2) site was fully occupied and oxygen vacancies were spread on the two
35 O(1) and O(3) equatorial sites. The model deduced from neutron diffraction was used to refine X-
36 ray diffraction data collected on the same composition, at the same temperature. As previously,
37 oxygen positions were maintained at the positions derived from neutron diffraction and only the
38 positions of heavy atoms were refined in this case. Close values were derived. The results of both
39 refinements are given in Table 2 and calculated data are compared to experimental data in Fig. 5.
40 A drawing of the Joint Probability Density Function (JPDF) of oxygen nucleons around the
41 indium atoms is given in Fig. 6. It represents the probability to find an oxygen atom around its
42
43
44
45
46
47
48
49
50
51
52
53
54
55
56
57
58
59
60
61
62
63
64
65

1
2
3
4 equilibrium position. A large disorder of the oxygen nuclear density is clearly observed around
5 the In(2) site, in contrast to the In(1) site. Oxygen vacancies are also mainly located in the In(2)
6 layers, although a few vacancies are observed in the In(1) layers. The presence of oxygen
7 vacancies in the In(1) layers is not surprising. Indeed, calculation of defect energy in the parent
8 compound, $\text{Ba}_2\text{In}_2\text{O}_5$, led to the conclusion that formation of Frenkel defect involving an oxygen
9 vacancy in the octahedral layers associated to an interstitial oxide in the tetrahedral layers of
10 $\text{Ba}_2\text{In}_2\text{O}_5$ was most favourable [24]. The increase of their concentration would explain the sudden
11 increase in conductivity observed for the parent compound at temperature higher than 925°C and
12 the transformation to the perovskite at 1040°C .
13
14
15
16
17
18
19
20

21 To derive preferential oxygen diffusion pathways in the molybdenum doped materials,
22 pseudo-potentials were calculated. Indeed the vibration of an atom around its equilibrium position
23 depends on the interactions bringing it back to its equilibrium position and these interactions can
24 be described by pseudo-potentials related to the probability of a given path [25]. From JPDF,
25 pseudo-potential can be calculated and allow to define preferred oxygen diffusion pathways.
26 These calculations were already applied to BIMEVOX compounds [26-27]. For data collected on
27 the parent compound, $\text{Bi}_4\text{V}_2\text{O}_{11}$, at 700°C , an energy barrier of 0.16eV was derived. It was in
28 good agreement with the experimental value measured by impedance spectroscopy. In the present
29 study, from the previous JPDF, numerous pathways were considered and the lowest energy
30 barriers were observed for the jump of an equatorial O(3) oxide to a consecutive equatorial O(3)
31 oxide in the In(2) layers with a value of 0.4eV . A value of 0.6eV was deduced for the jump of an
32 apical site to an equatorial site in the same layers. Since oxygen vacancies were also evidenced in
33 the In(1) layers, one could expect the possibility of oxygen motion in these layers. The lowest
34 energy barrier in these In(1) layers was deduced for the jump of an apical O(1) site to an adjacent
35 apical O(1) site with a barrier of 3.9eV . Jumps from an equatorial site to an apical site in the same
36 layers were also considered but appeared to be not possible. In summary, the most probable
37 pathway for oxygen ions (i.e. having the lowest potential) is in the In(2) layers from an equatorial
38 to an equatorial site with an activation energy of 0.4eV . And therefore, an activation energy of
39 0.4eV would be expected for the present composition at 700°C . However, a value of 1eV was
40 derived from impedance spectroscopy. In fact, these pseudo-potentials have to be used with care.
41 They only give qualitative information on the possibility of oxide migration and suppose a
42 dynamic disorder of atoms. Indeed, one can not exclude the possibility that the nuclear density
43
44
45
46
47
48
49
50
51
52
53
54
55
56
57
58
59
60
61
62
63
64
65

1
2
3
4 spreading evidenced at this temperature for the present composition would be the result of the
5 superimposition of different oxygen surrounding of indium atoms instead of a dynamic disorder.
6 This is even more likely that 700°C is very close to the transition of phase from the orthorhombic
7 to the tetragonal form.
8
9

10 11 12 3.3. Composition $x=0.1$ at 950°C 13

14
15 At 950°C, both X-ray and neutron diffraction revealed a cubic symmetry. The structure
16 was refined in the $Pm\bar{3}m$ space group using the model of the perovskite. Isotropic displacement
17 parameters were used to describe the thermal motions of barium, indium, and molybdenum
18 atoms. In contrast, an anharmonic tensor of the 4th order was used for oxygen atoms. Results of
19 the refinement of X-ray and neutron data are given in Table 3 and calculated data are compared to
20 experimental data in Fig. 7. The model was confirmed using data collected at $\lambda\sim 1.05$ Å. Only
21 data collected at $\lambda\sim 1.6$ Å are presented here since the D2B diffractometer is optimized for $\lambda\sim 1.6$
22 Å and consequently the resolution is better for this wavelength. The three dimensions plot of the
23 JPDF of oxygen nucleon is reported in Fig. 8. When considering the jump of an oxygen atom to
24 an adjacent one, an energy barrier of 1.1eV was deduced in agreement with the experimental
25 value of 1eV obtained by impedance spectroscopy in the domain of temperature. The disorder
26 observed at this temperature is likely dynamic which allows the comparison in this case [25].
27
28
29
30
31
32
33
34
35
36
37

38 3.4. Composition $x=0.5$ at room temperature and at 750°C 39

40
41 For composition $x=0.5$, a cubic form was stabilized at room temperature. Data were
42 collected at room temperature and at 750°C. The refinements of neutron diffraction data only are
43 reported. Since the wavelength of neutron had been changed between two measurements, it was
44 refined again with the unit cell parameters constrained to the values obtained from X-ray
45 diffraction at room temperature. This led to a value of $\lambda=1.59599(3)$ Å. Then, the model of the
46 cubic perovskite was introduced. Isotropic displacement parameters were used to describe the
47 thermal motions of barium, indium, molybdenum, and anharmonic tensors of the 4th order to
48 describe those of oxygen atoms. Results of the refinements are given in Table 4 and 5. The 3D
49 plot of the JPDF for oxygen nucleon at room temperature is compared to JPDF for oxygen
50 nucleon at 750°C in Fig. 11. At 750°C, it is similar to the JPDF observed at 950°C for $x=0.1$. At
51 room temperature, the nucleon density of oxide ions is split. These shapes are unlikely due to
52
53
54
55
56
57
58
59
60
61
62
63
64
65

1
2
3
4 thermal motion, but are more probably the result of the superimposition of different local
5 environments around the molybdenum and indium atoms with two different bond lengths equal to
6 1.88Å and 2.29Å. An EXAFS study at the L_{III} edge of tungsten and L_I edge of indium in tungsten
7 doped derivatives revealed for cubic forms two different In-O bond lengths in good proportion
8 with the tungsten amount indicating different oxygen surrounding for indium atoms whether it is
9 close to a tungsten atom or not [28]. No superlattice reflection was revealed by TEM, indicating a
10 perfect solution of tungsten in the structure. This scenario is likely the same for Mo-doped
11 compounds.
12
13
14
15
16
17
18
19
20
21

22 **5. Conclusions**

23
24
25 To derive preferred oxygen diffusion pathways, the structures of molybdenum doped
26 $Ba_2In_2O_5$ were refined from X-ray and neutron diffraction data at room and high temperature. At
27 room temperature, refinement of composition $Ba_2In_{2-x}Mo_xO_{5+3x/2}$ with $x=0.1$ revealed
28 molybdenum atoms to be preferentially located in the tetrahedral layers of $Ba_2In_2O_5$. At 700°C,
29 the structure can be viewed as the stacking of alternating In and In/Mo octahedral layers. The
30 conduction process occurs preferentially in the later which is highly oxygen deficient. Preferred
31 oxygen pathways were deduced from Joint Probability Density Function (JPDF) and energy
32 barriers were derived. It was in good agreement with the activation energy deduced from
33 impedance spectroscopy for composition $x=0.1$ at 950°C. However, calculation of energy barrier
34 assumes a dynamic disorder of oxide ion which is unlikely at lower temperature and for sample
35 containing a larger amount of molybdenum. Composition $x=0.5$ is cubic on the whole range of
36 temperature. At room temperature, JPDF revealed a static disorder of the oxygen atoms likely due
37 to the solution of molybdenum into the barium indium perovskite. When temperature increases
38 the disorder becomes more and more dynamic.
39
40
41
42
43
44
45
46
47
48
49
50
51
52
53
54
55
56
57
58
59
60
61
62
63
64
65

1
2
3
4 **Acknowledgements**
5
6

7 The Institut Laue Langevin is thanked for providing neutron facilities. The authors are
8 also very grateful to L. Burylo and N. Djelal for help with the X-ray diffraction and EDX
9 analysis. The Fonds Européen de Développement Régional (FEDER), the Centre National de la
10 Recherche Scientifique (CNRS), the Région Nord Pas-de-Calais and the Ministère de l'Education
11 Nationale, de l'Enseignement Supérieur et de la Recherche are acknowledged for funding of X-
12 ray diffractometers. Aurelie Rolle is also very grateful to the CNRS and the Région Nord Pas-de-
13 Calais for funding her PhD.
14
15
16
17
18
19
20
21
22

23 **References**
24

- 25
26 [1] J. B Goodenough, J. E Ruiz-Diaz, Y.S. Zhen, *Solid State Ionics* 44 (1990) 21.
27
28 [2] P. Berastegui, S. Hull, F.J. García-García, S.G. Eriksson, *J. Solid State Chem.* 164 (2002) 119.
29
30 [3] T.R.S. Prasanna, A. Navrotsky, *J. Mater. Res.* 8 (1993) 1484.
31
32 [4] S. B. Adler, J.A. Reimer, J. Baltisberger, U. Werner, *J. Am. Chem. Soc.* 116 (1994) 675.
33
34 [5] G. B. Zhang, D. M. Smyth, *Solid State Ionics* 82 (1995) 161.
35
36 [6] M. Kanzaki, A. Yamaji, *Mater. Sci Eng.* B41 (1996) 46.
37
38 [7] T. Hashimoto, Y.Ueda, M. Yoshinaga, K. Komazaki, K. Asaoka, S. Wang, *J. Electrochem.*
39 *Soc.* 149 (2002) 1381.
40
41 [8] T. Hashimoto, K. Asaoka, K. Komazaki, Y. Ueda Y, M. Yoshinaga, *Electrochemical Society*
42 *Proceedings* 28 (2001) 291.
43
44 [9] S.A. Speakman, J.W. Richardson, B.J. Mitchell, S.T. Mixture, *Solid State Ionics* 149 (2002)
45 247.
46
47 [10] A. Rolle, N.V. Giridharan, R.N. Vannier, F. Abraham, *Solid State Ionics* 176 (2005) 2095.
48
49
50
51
52
53
54
55
56
57
58
59
60
61
62
63
64
65

- 1
2
3
4 [11] A. Rolle, N.V. Giridharan, P. Roussel, F. Abraham, R.N. Vannier, *MRS Symposium*
5 *Proceedings* (2005) 835, K.2.4.1.
6
7
8 [12] V. Petricek, M. Dusek, *The crystallographic computing system JANA 2000*; Institute of
9 Physics: Praha, Czech Republic, 2006.
10
11
12 [13] Eck B., *wxDragon*; Institut für Anorganische Chemie der RWTH: Aachen, Germany, 2006.
13
14
15 [14] D.H. Gregory, M.T.Weller, *J. Solid State Chem.* 107 (1993) 134.
16
17
18 [15] C. Greaves, A.J. Jacobson, B.C. Tofield , B.E.F. Fender, *Acta Crystallogr. Sect B* 31 (1975)
19 641.
20
21
22 [16] C. Tenailleau, A. Pring, S.M. Moussa, Y. Liu, R.L. Withers, S. Tarantino, M. Zhang, A.
23 Carpenter, *J. Solid State Chem.* 178 (2005) 882.
24
25
26 [17] A.L. Kharlanov, *Russian J. Inorg. Chem.* 35(12) (1990) 1741.
27
28
29 [18] G. Kallias, M. Pissas, A. Simopoulos, D. Niarchos, *Mater. Res. Bull.* 32(6) (1997) 791.
30
31
32 [19] A.K. Ganguli , T.N. Guru Row, *Mater. Res. Bull.* 29(12) 1994 1333.
33
34
35 [20] V. Jayaraman , A. Magrez, M. Caldes, O. Joubert, M. Ganne, Y. Piffard, L. Brohan, *Solid*
36 *State Ionics* 170 (2004) 17.
37
38
39 [21] Y. Liu, R.L. Withers, J.F. Gerald, *J. Solid State Chem.* 170 (2003) 247.
40
41
42 [22] S. Kambe, I. Shime, S. Ohshima, K. Okuyama, N. Ohnishi, K. Hiraga, *Physica C* 220 (1994)
43 119.
44
45
46 [23] W.C. Hamilton, *Acta Cryst.* 18 (1965) 502.
47
48
49 [24] A. Rolle, C.A.J. Fisher, R.N. Vannier, M.S. Islam, to be submitted.
50
51
52 [25] R. Bachman, H. Schulz, *Acta Crystallogr. Sect. A* 40 (1984) 668.
53
54
55 [26] P. Roussel, R.N. Vannier, M. Anne, G. Nowogrocki, G. Mairesse, *Acta Crystallogr. Sect. A*
56 58 (2002) C319.
57
58
59 [27] P. Roussel, R.N. Vannier, M. Anne, G. Nowogrocki, G. Mairesse, to be submitted.
60
61
62
63
64
65

1
2
3
4 [28] S. Daviero-Minaud, A. Rolle, C. Kongmark, R.N. Vannier, “X-ray absorption study of
5
6 $Ba_2In_{2-x}W_xO_{5+3x/2}$ compounds”, to be submitted.
7
8
9

10
11 **Table captions**
12
13

14 Table 1. Structural model of $Ba_2In_{2-x}Mo_xO_{5+3x/2}$ ($x=0.1$) described in the $Icmm$ space group
15 deduced from the refinement of neutron and X-ray diffraction data collected at room temperature
16
17 ($\lambda=1.59483(2)\text{\AA}$)
18
19

20 Table 2. Structural model of $Ba_2In_{2-x}Mo_xO_{5+3x/2}$ ($x=0.1$) described in the $P4/mmm$ space group
21 deduced from the refinement of neutron and X-ray diffraction data collected at 700°C
22
23 ($\lambda=1.59483(2)\text{\AA}$)
24
25

26 Table 3. Structural model of $Ba_2In_{2-x}Mo_xO_{5+3x/2}$ ($x=0.1$) described in the $Pm\bar{3}m$ space group
27 deduced from the refinement of neutron and X-ray diffraction data collected at 950°C
28
29 ($\lambda=1.59483(2)\text{\AA}$)
30
31
32

33 Table 4. Structural model of $Ba_2In_{2-x}Mo_xO_{5+3x/2}$ ($x=0.5$) described in the $Pm\bar{3}m$ space group
34 deduced from the refinement of neutron and X-ray diffraction data collected at room temperature
35
36 ($\lambda=1.59599(3)\text{\AA}$)
37
38
39

40 Table 5. Structural model of $Ba_2In_{2-x}Mo_xO_{5+3x/2}$ ($x=0.5$) described in the $Pm\bar{3}m$ space group
41 deduced from the refinement of neutron data collected at 750°C ($\lambda=1.59599(3)\text{\AA}$)
42
43
44
45
46
47
48
49
50
51
52
53
54
55
56
57
58
59
60
61
62
63
64
65

1
2
3
4 **Tables**
5
6

7 Table 1

8
9 Structural model of Ba₂In_{2-x}Mo_xO_{5+3x/2} (x=0.1) described in the *Icmm* space group deduced from
10 the refinement of neutron and X-ray diffraction data collected at room temperature
11 (λ=1.59483(2)Å)
12
13
14

15
16
17

<i>Icmm</i>	a (Å)	b (Å)	c (Å)	volume (Å ³)	density
	6.0293(6)	16.822(2)	5.9616(6)	604.7(2)	6.5(1)

18
19
20
21
22
23
24

25

atom	site	diffraction	x	y	z	occupancy	U _{iso} (Å ²)
Ba	8(h)	neutron	0.508(1)	0.6111(2)	0	1	0.0112(9)
		X-ray	0.5058(9)	0.612(1)	0	1	0.005(1)
In(1)	4(a)	neutron	0	0	0	1	0.005(1)
		X-ray	0	0	0	1	0.003(2)
In(2)/Mo(2)	8(i)	neutron	0.547(2)	0.25	0.477(6)	0.45/0.05	0.026(4)
		X-ray	0.541(1)	0.25	0.480(6)	0.45/0.05	0.014(3)
O(1)	8(g)	neutron	0.25	0.9957(4)	0.25	0.995(6)	0.0147(8)
		X-ray	0.25	0.9957	0.25	0.995	0.0147
O(2)	8(h)	neutron	0.037(1)	0.1360(3)	0	1	0.038(1)
		X-ray	0.037	0.1360	0	1	0.038
O(3)	8(i)	neutron	0.649(2)	0.25	0.152(2)	0.483(4)	0.031(3)
		X-ray	0.649	0.25	0.152	0.483	0.031
O(4)	4(c)	neutron	0.25	0.25	0.25	0.194(4)	0.05(1)
		X-ray	0.25	0.25	0.25	0.194	0.05

26
27
28
29
30
31
32
33
34
35
36
37
38
39
40
41
42
43
44
45
46
47
48
49
50
51
52
53
54
55
56
57
58
59
60
61
62
63
64
65

Table 2

Structural model of $\text{Ba}_2\text{In}_{2-x}\text{Mo}_x\text{O}_{5+3x/2}$ ($x=0.1$) described in the $P4/mmm$ space group deduced from the refinement of neutron and X-ray diffraction data collected at 700°C ($\lambda=1.59483(2)\text{\AA}$)

<i>P4/mmm</i>	a (Å)	b (Å)	c (Å)	volume (Å ³)	density
neutrons	4.2589(3)	4.2589(3)	8.5234(5)	154.60(1)	6.2797(3)
X rays	4.2589(3)	4.2589(3)	8.5202(2)	154.54(2)	6.2820(8)

atom	site	diffraction	x	y	z	occupancy	U_{eq} (Å ²)
Ba	2(h)	neutrons	0.5	0.5	0.2348(6)	1	0.050(2)*
		X rays	0.5	0.5	0.230(1)	1	0.016(8)*
In(1)	(1a)	neutrons	0	0	0	1	0.03(6)*
		X rays	0	0	0	1	0.02(2)*
In(2)/Mo(2)	(1b)	neutrons	0	0	0.5	0.9/0.1	0.089(5)*
		X rays	0	0	0.5	0.9/0.1	0.04(3)*
O(1)	(2f)	neutrons	0.5	0	0	0.935(7)	0.056(3)*
		X rays	0.5	0	0	0.935	0.056*
O(2)	(2g)	neutrons	0	0	0.268(1)	1	0.179(8)**
		X rays	0	0	0.268	1	0.179**
O(3)	(2e)	neutrons	0.5	0	0.5	0.640(4)	0.53(5)**
		X rays	0.5	0	0.5	0.640	0.53**

* U_{aniso}		U_{11}	U_{22}	U_{33}	U_{12}	U_{13}	U_{23}
Ba	neutrons	0.07(3)	0.07(3)	0.006(3)	0	0	0
	X rays	0.02(1)	0.02(1)	0.01(2)	0	0	0
In(1)	neutrons	0.0257(5)	0.0257(5)	0.0520(4)	0	0	0
	X rays	0.01(2)	0.01(2)	0.03(5)	0	0	0
In(2)	neutrons	0.14(1)	0.14(1)	0.008(3)	0	0	0
	X rays	0.05(2)	0.05(2)	0.02(5)	0	0	0
Mo(2)	neutrons	0.14(1)	0.14(1)	0.008(3)	0	0	0
	X rays	0.05(2)	0.05(2)	0.02(5)	0	0	0
O(1)	neutrons	0.042(5)	0.048(5)	0.078(7)	0	0	0
	X rays	0.042	0.048	0.078	0	0	0

** U_{anharm}		U_{11}	U_{22}	U_{33}	U_{12}	U_{13}	U_{23}
O(2)	neutrons	0.27(1)	0.27(1)	0.012(5)	0	0	0
	X rays	0.27	0.27	0.012	0	0	0
O(3)	neutrons	0.11(2)	1.4(1)	0.10(2)	0	0	0
	X rays	0.11	1.4	0.10	0	0	0

* an anisotropic description of the thermal parameter was used

** an anharmonic description of the thermal parameters at the 4th order was used

Table 3

Structural model of $\text{Ba}_2\text{In}_{2-x}\text{Mo}_x\text{O}_{5+3x/2}$ ($x=0.1$) described in the $Pm\bar{3}m$ space group deduced from the refinement of neutron and X-ray diffraction data collected at 950°C ($\lambda=1.59483(2)\text{\AA}$)

$Pm\bar{3}m$	a (\AA)	b (\AA)	c (\AA)	volume (\AA^3)	density
neutrons	4.2706(1)	4.2706(1)	4.2706(1)	77.855(2)	6.2324(1)
X rays	4.2699(1)	4.2699(1)	4.2699(1)	77.852(3)	6.2350(3)

atom	site	diffraction	x	y	z	occupancy	U_{iso} (\AA^2)
Ba	1(b)	neutrons	0.5	0.5	0.5	1	0.055(1)
		X rays	0.5	0.5	0.5	1	0.030(6)
In/Mo	(1a)	neutrons	0	0	0	0.95/0.05	0.051(1)
		X rays	0	0	0	0.95/0.05	0.030(8)
O(1)	3(f)	neutrons	0	0	0.5	0.86	0.10(3)**
		X rays	0	0	0.5	0.86	0.102

** U_{anharm}	U_{11}	U_{22}	U_{33}	U_{12}	U_{13}	U_{23}
O	0.120(3)	0.120(3)	0.066(3)	0	0	0

Table 4

Structural model of $\text{Ba}_2\text{In}_{2-x}\text{Mo}_x\text{O}_{5+3x/2}$ ($x=0.5$) described in the $Pm\bar{3}m$ space group deduced from the refinement of neutron and X-ray diffraction data collected at room temperature ($\lambda=1.59599(3)$ Å)

$Pm\bar{3}m$	a (Å)	b (Å)	c (Å)	volume (Å ³)	density
neutrons	4.1765	4.1765	4.1765	72.853	6.6861
X rays	4.1765(2)	4.1765(2)	4.1765(2)	72.853(4)	6.6861(3)

atom	site	diffraction	x	y	z	occupancy	U_{iso} (Å ²)
Ba	1(b)	neutrons	0.5	0.5	0.5	1	0.0148(2)
		X rays	0.5	0.5	0.5	1	0.0148
In/Mo	(1a)	neutrons	0	0	0	0.75/0.25	0.0094(2)
		X rays	0	0	0	0.75/0.25	0.0094
O(1)	3(f)	neutrons	0	0	0.5	0.96	0.033(1)**
		X rays	0	0	0.5	0.96	0.033**

** U_{anharm}	U_{11}	U_{22}	U_{33}	U_{12}	U_{13}	U_{23}
O	0.037(1)	0.037(1)	0.026(2)	0	0	0

Table 5

Structural model of $\text{Ba}_2\text{In}_{2-x}\text{Mo}_x\text{O}_{5+3x/2}$ ($x=0.5$) described in the $Pm\bar{3}m$ space group deduced from the refinement of neutron data collected at 750°C

$Pm\bar{3}m$	a (Å)	b (Å)	c (Å)	volume (Å ³)	density
neutrons	4.21671(4)	4.21671(4)	4.21671(4)	74.9763(8)	6.49672(7)

atom	site	diffraction	x	y	z	occupancy	U_{iso} (Å ²)
Ba	1(b)	neutrons	0.5	0.5	0.5	1	0.0343(4)
In/Mo	1(a)	neutrons	0	0	0	0.75/0.25	0.0244(4)
O	3(d)	neutrons	0	0	0.5	0.96	0.0559(9)**

** U_{anharm}	U_{11}	U_{22}	U_{33}	U_{12}	U_{13}	U_{23}
O	0.063(1)	0.063(1)	0.043(1)	0	0	0

Figure captions

Fig. 1. Arrhenius plot of $\text{Ba}_2\text{In}_{2-x}\text{Mo}_x\text{O}_{5+3x/2}$ with $x=0, 0.1, 0.5$

Fig. 2. Description of the crystal structure of $\text{Ba}_2\text{In}_2\text{O}_5$ in the a) $Pcmn$ and b) $Ibm2$ space groups

Fig. 3. In(2) surrounding in the average structural model of $\text{Ba}_2\text{In}_2\text{O}_5$ described in the $Icmm$ space group. In(2) and O(3) are split sites which are partially occupied. This splitting corresponds to two different configurations, one set is represented in black with full lines for bond length, the other is given in grey with dashed lines for bond length.

Fig. 4. Calculated profile compared to experimental data (neutron (a) and X-ray (b) diffraction data) of $\text{Ba}_2\text{In}_{2-x}\text{Mo}_x\text{O}_{5+3x/2}$ $x=0.1$ obtained at room temperature

Fig. 5. Calculated profile compared to experimental data (neutron (a) and X-ray (b) diffraction data) of $\text{Ba}_2\text{In}_{2-x}\text{Mo}_x\text{O}_{5+3x/2}$ $x=0.1$ obtained at 700°C

1
2
3
4 Fig. 6. 3D plot drawing of the Joint Probability Density Function of oxygen nucleons around the
5 indium atoms in case of $\text{Ba}_2\text{In}_{2-x}\text{Mo}_x\text{O}_{5+3x/2}$ $x=0.1$ obtained at 700°C
6
7

8 Fig. 7. Calculated profile compared to experimental data (neutron (a) and X-ray (b) diffraction
9 data) of $\text{Ba}_2\text{In}_{2-x}\text{Mo}_x\text{O}_{5+3x/2}$ $x=0.1$ collected at 950°C
10
11

12 Fig. 8. Drawing of the Joint Probability Density Function of oxygen nucleons around the indium
13 atoms in case of $\text{Ba}_2\text{In}_{2-x}\text{Mo}_x\text{O}_{5+3x/2}$ $x=0.1$ collected at 950°C
14
15

16 Fig. 9. Calculated profile compared to experimental data (neutron (a) and diffraction (b) data) of
17 $\text{Ba}_2\text{In}_{2-x}\text{Mo}_x\text{O}_{5+3x/2}$ $x=0.5$ collected at room temperature
18
19

20 Fig. 10. Calculated profile compared to experimental neutron data of $\text{Ba}_2\text{In}_{2-x}\text{Mo}_x\text{O}_{5+3x/2}$ $x=0.5$
21 obtained at 750°C
22
23

24 Fig. 11. Drawing of the Joint Probability Density Function of oxygen nucleons around the indium
25 atoms in case of $\text{Ba}_2\text{In}_{2-x}\text{Mo}_x\text{O}_{5+3x/2}$ $x=0.5$ obtained at room temperature (a) and at 750°C (b).
26
27
28
29
30
31
32
33
34
35
36
37
38
39
40
41
42
43
44
45
46
47
48
49
50
51
52
53
54
55
56
57
58
59
60
61
62
63
64
65

Figures

Fig. 1. Arrhenius plot of $\text{Ba}_2\text{In}_{2-x}\text{Mo}_x\text{O}_{5+3x/2}$ with $x=0, 0.1, 0.5$

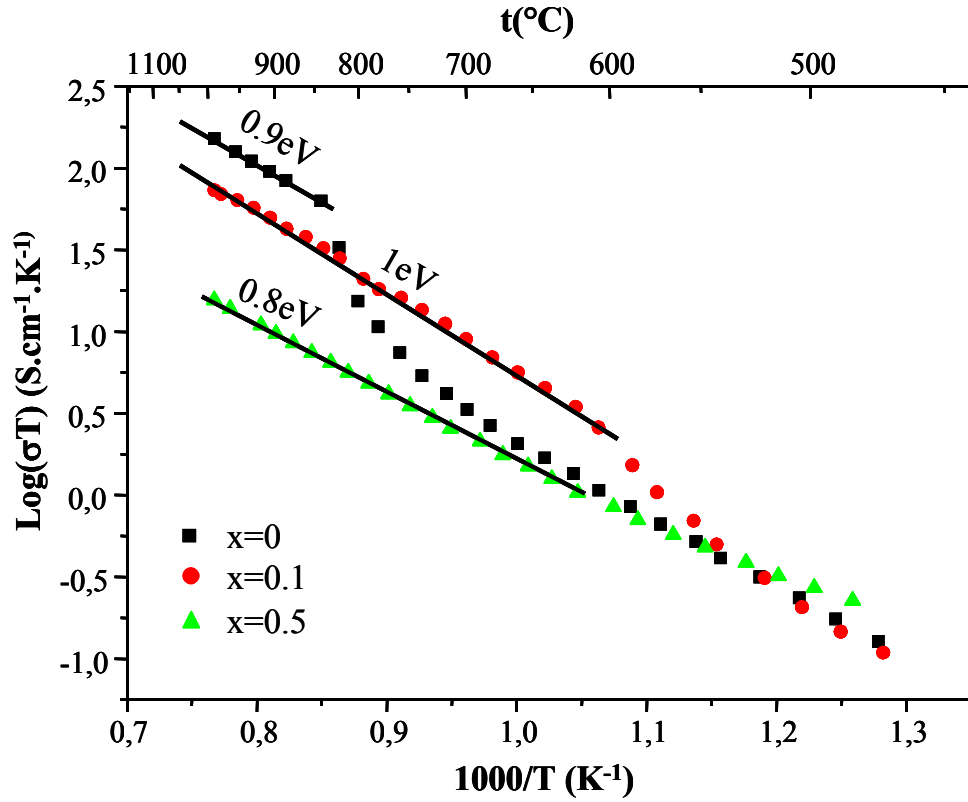
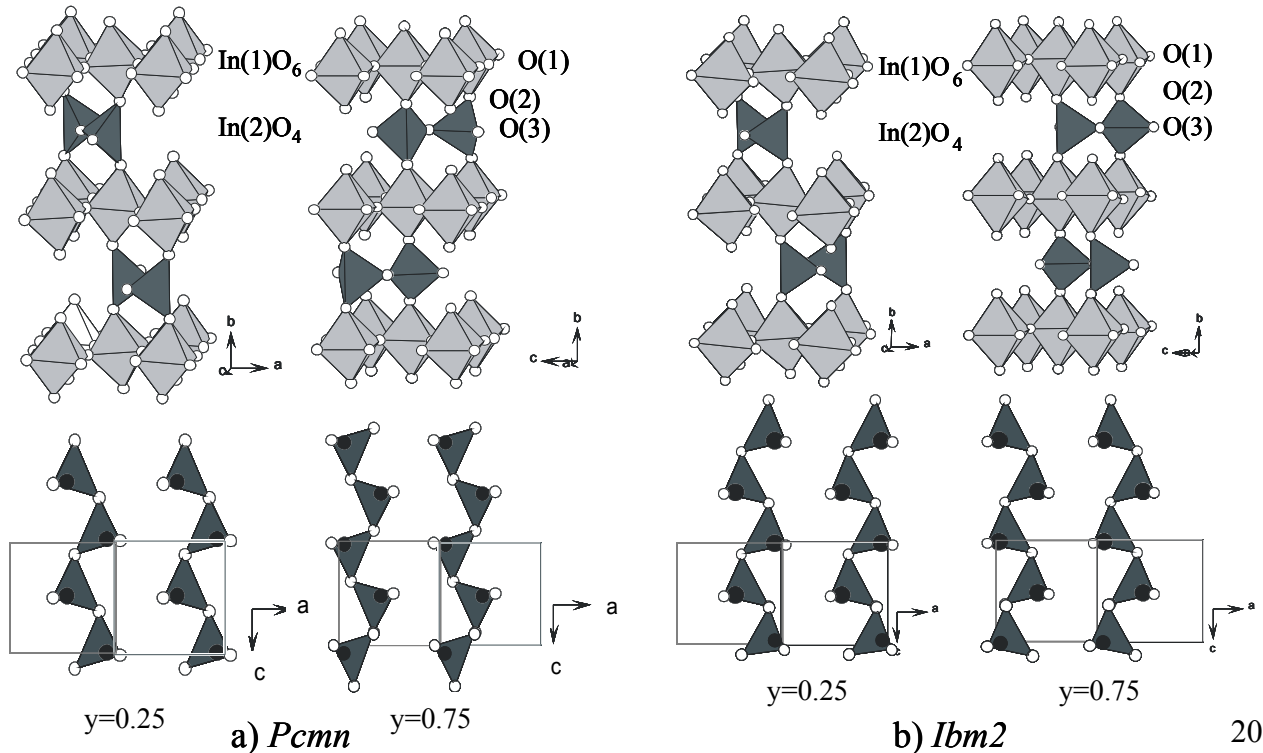


Fig. 2. Description of the crystal structure of $\text{Ba}_2\text{In}_2\text{O}_5$ in the a) *Pcmn* and b) *Ibm2* space groups



1
2
3
4
5
6
7
8
9
10
11
12
13
14
15
16
17
18
19
20
21
22
23
24
25
26
27
28
29
30
31
32
33
34
35
36
37
38
39
40
41
42
43
44
45
46
47
48
49
50
51
52
53
54
55
56
57
58
59
60
61
62
63
64
65

Fig. 3. In(2) surrounding in the average structural model of $\text{Ba}_2\text{In}_2\text{O}_5$ described in the $Icmm$ space group. In(2) and O(3) are split sites which are partially occupied. This splitting corresponds to two different configurations, one set is represented in black with full lines for bond length, the other is given in grey with dashed lines for bond length.

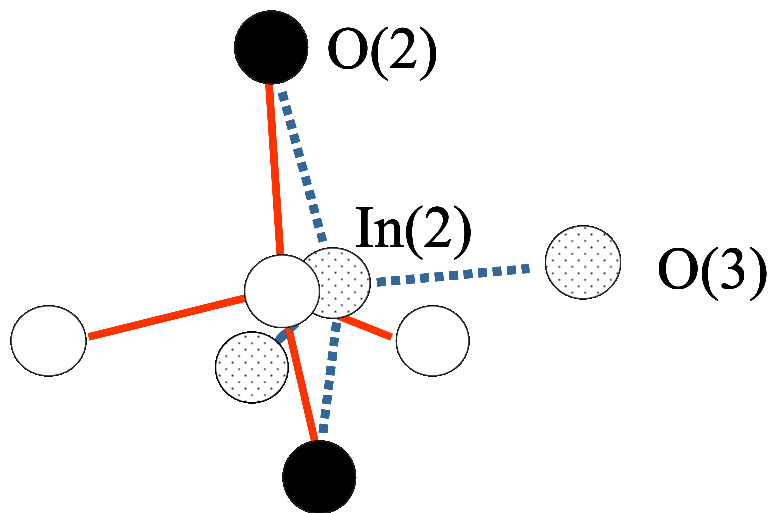
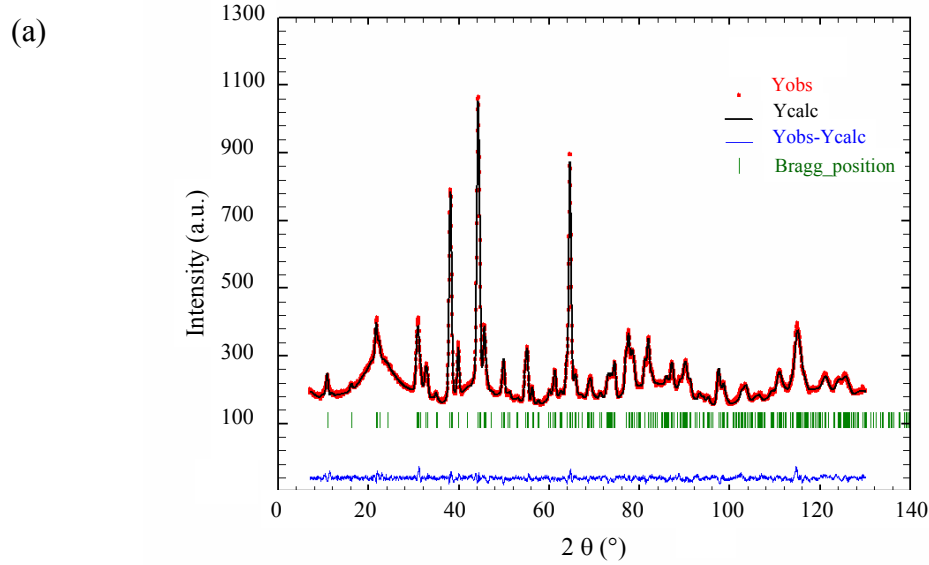
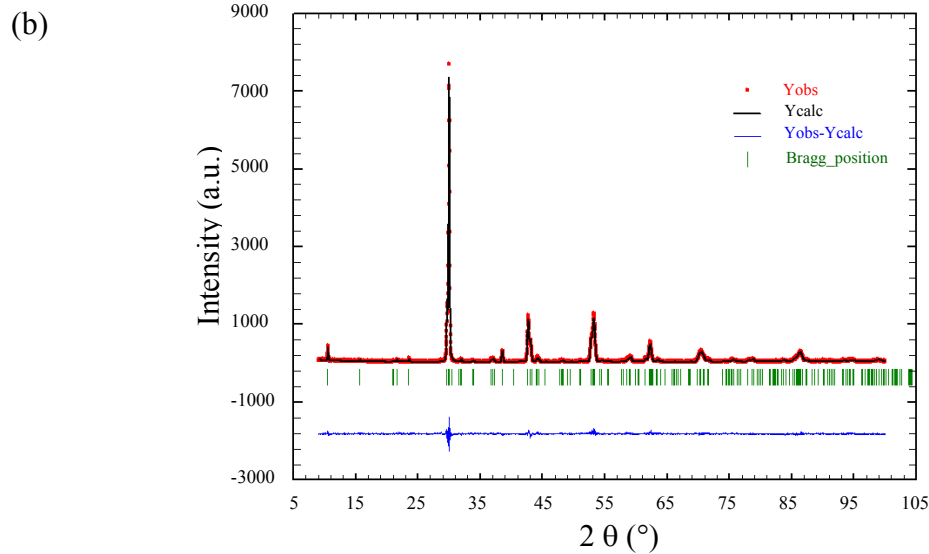


Fig. 4. Calculated profile compared to experimental data (neutron (a) and X-ray (b) diffraction data) of $\text{Ba}_2\text{In}_{2-x}\text{Mo}_x\text{O}_{5+3x/2}$ $x=0.1$ collected at room temperature



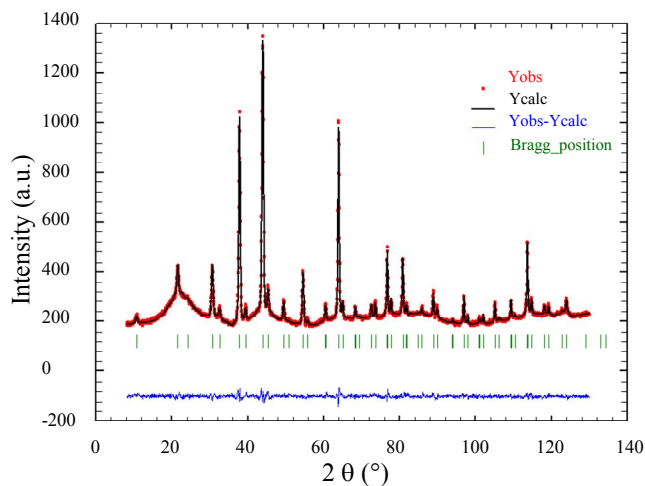
R_{obs}	R_{wobs}	R_{all}	R_{wall}	R_{p}	R_{wp}	R_{exp}
2.94	2.26	2.95	2.26	1.86	2.37	1.59



R_{obs}	R_{wobs}	R_{all}	R_{wall}	R_{p}	R_{wp}	R_{exp}
4.63	3.21	4.94	3.22	9.32	12.65	10.08

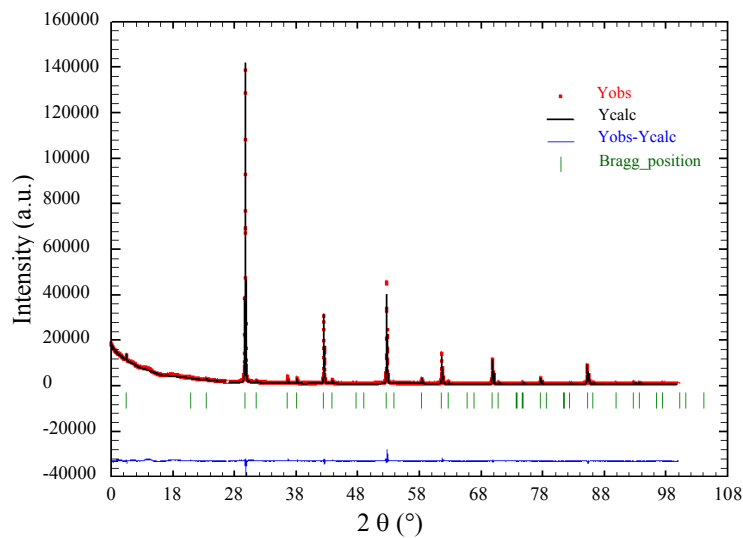
Figure 5. Calculated profile compared to experimental data (neutron (a) and X-ray (b) diffraction data) of $\text{Ba}_2\text{In}_{2-x}\text{Mo}_x\text{O}_{5+3x/2}$ $x=0.1$ collected at 700°C

(a)



R_{obs}	R_{wobs}	R_{all}	R_{wall}	R_{p}	R_{wp}	R_{exp}
2.55	1.39	2.71	1.40	1.67	2.12	1.56

(b)



R_{obs}	R_{wobs}	R_{all}	R_{wall}	R_{p}	R_{wp}	R_{exp}
6.29	3.16	7.00	3.17	4.34	5.99	2.06

Fig. 6. 3D plot drawing of the Joint Probability Density Function of oxygen nucleons around the indium atoms in case of $\text{Ba}_2\text{In}_{2-x}\text{Mo}_x\text{O}_{5+3x/2}$ $x=0.1$ collected at 700°C

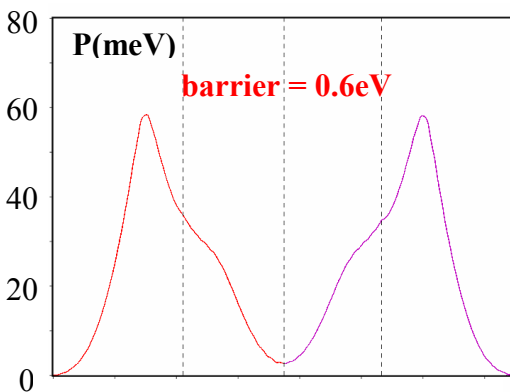
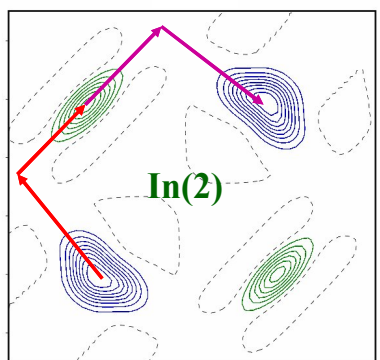
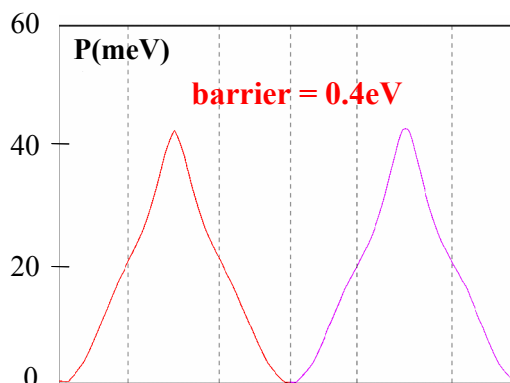
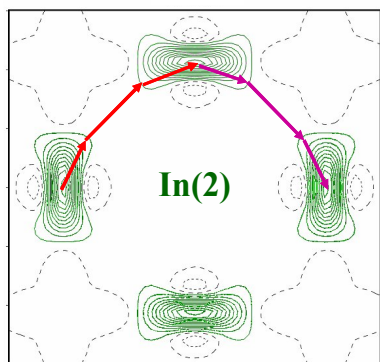
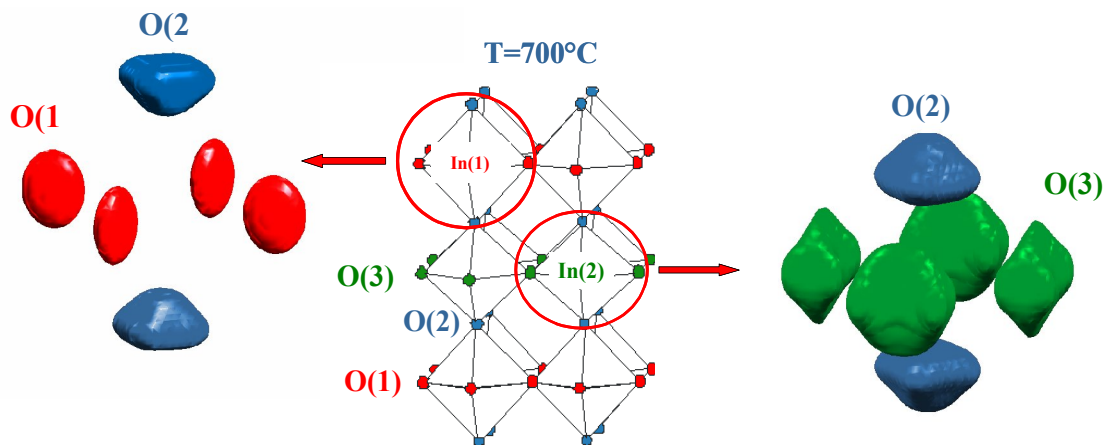
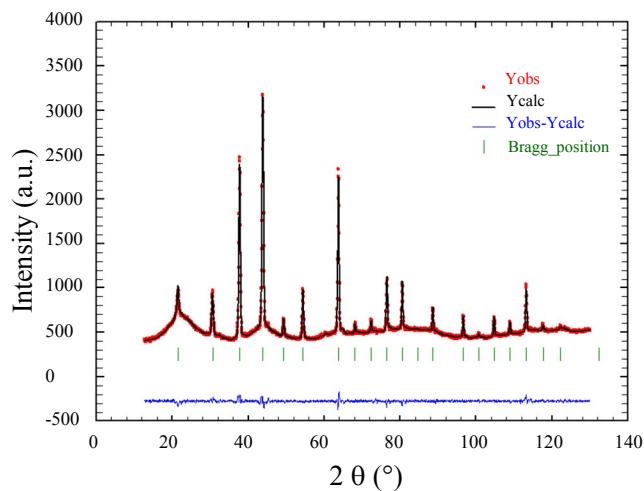


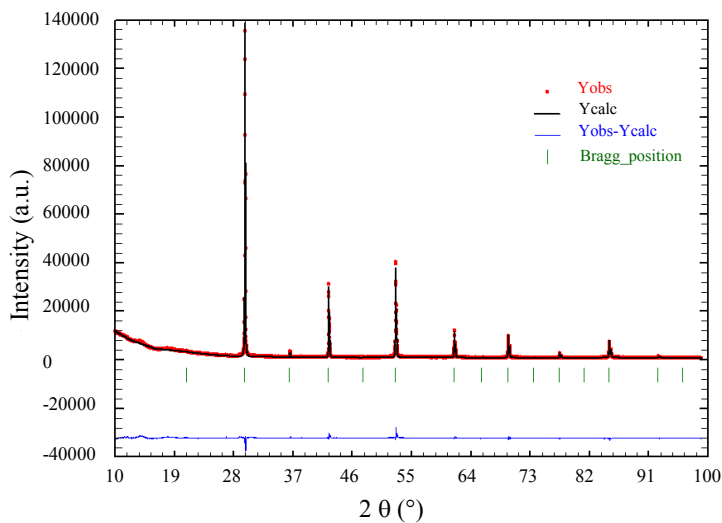
Fig. 7. Calculated profile compared to experimental data (neutron (a) and X-ray (b) diffraction data) of $\text{Ba}_2\text{In}_{2-x}\text{Mo}_x\text{O}_{5+3x/2}$ $x=0.1$ collected at 950°C

(a)



R_{obs}	R_{wobs}	R_{all}	R_{wall}	R_{p}	R_{wp}	R_{exp}
1.85	1.68	2.21	1.69	1.51	2.00	1.43

(b)



R_{obs}	R_{wobs}	R_{all}	R_{wall}	R_{p}	R_{wp}	R_{exp}
4.80	2.87	6.30	2.88	4.53	6.26	2.14

Fig. 8. Drawing of the Joint Probability Density Function of oxygen nucleons around the indium atoms in case of $\text{Ba}_2\text{In}_{2-x}\text{Mo}_x\text{O}_{5+3x/2}$ $x=0.1$ collected at 950°C

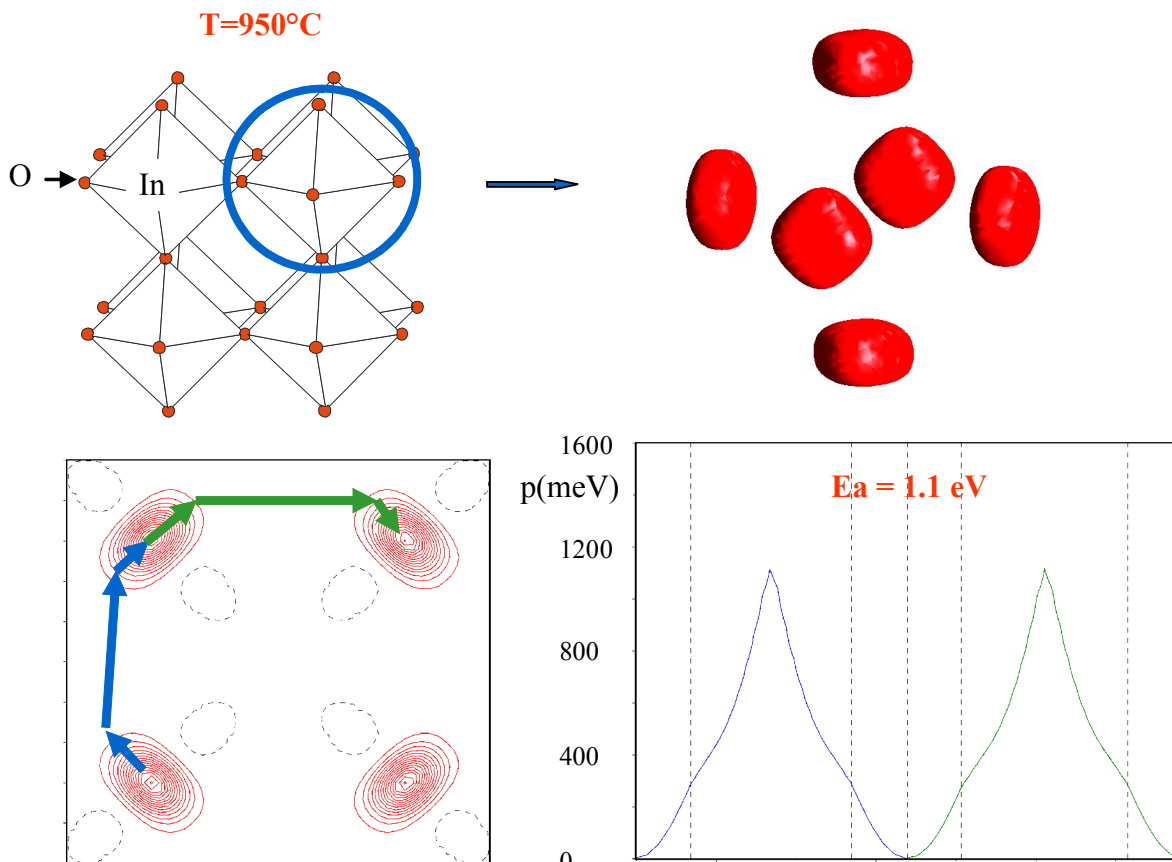
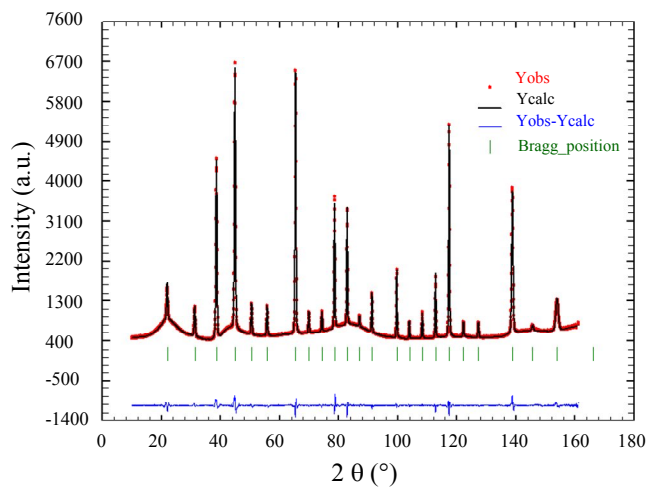


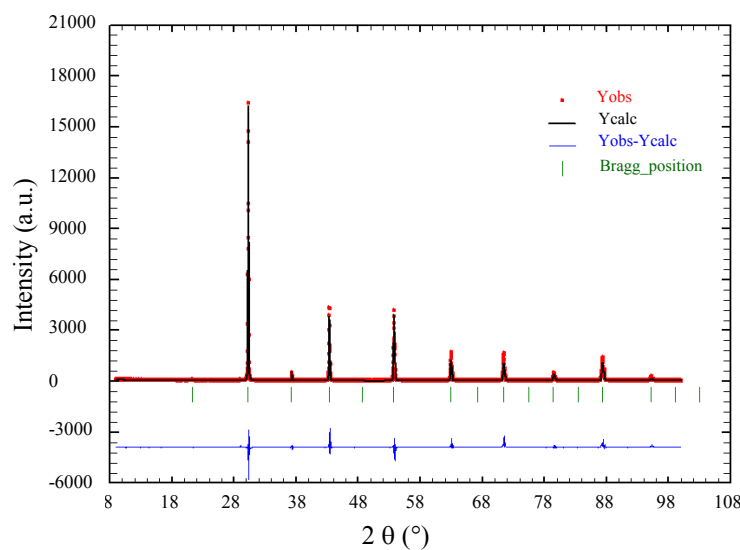
Fig. 9. Calculated profile compared to experimental data (neutron (a) and diffraction (b) data) of $\text{Ba}_2\text{In}_{2-x}\text{Mo}_x\text{O}_{5+3x/2}$ $x=0.5$ collected at room temperature

(a)



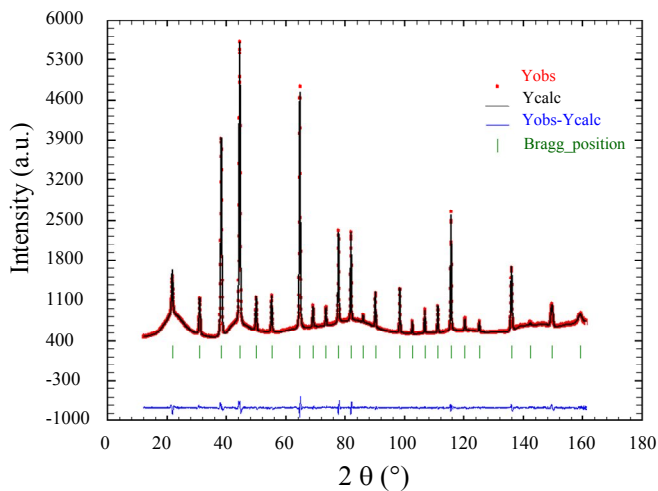
R_{obs}	R_{wobs}	R_{all}	R_{wall}	R_{p}	R_{wp}	R_{exp}
1.10	1.15	1.10	1.15	1.70	2.51	0.92

(b)



R_{obs}	R_{wobs}	R_{all}	R_{wall}	R_{p}	R_{wp}	R_{exp}
6.72	5.34	6.85	5.34	14.28	18.15	9.95

Fig. 10. Calculated profile compared to experimental neutron data of $\text{Ba}_2\text{In}_{2-x}\text{Mo}_x\text{O}_{5+3x/2}$ $x=0.5$ collected at 750°C



R_{obs}	R_{wobs}	R_{all}	R_{wall}	R_{p}	R_{wp}	R_{exp}
0.94	0.86	0.94	0.86	1.24	1.79	0.92

Fig. 11. Drawing of the Joint Probability Density Function of oxygen nucleons around the indium atoms in case of $\text{Ba}_2\text{In}_{2-x}\text{Mo}_x\text{O}_{5+3x/2}$ $x=0.5$ obtained at room temperature (a) and at 750°C (b).

